On the mechanism of the sensitization of PADC (poly(allyl diglycol carbonate)) track detectors by carbon dioxide treatment

Hassan, Nabil M. ; Matai, Yuri ; Kusumoto, Tamon ; Mori, Yutaka ; Kanasaki, Masato ; Oda, Keiji ; Kitamura, Hisashi ; Konishi, Teruaki ;…

(Citation)
Radiation Measurements,59:23-29

(Issue Date)
2013-12

(Resource Type)
journal article

(Version)
Accepted Manuscript

(URL)
https://hdl.handle.net/20.500.14094/90005200

On the mechanism of the sensitization of PADC (poly(allyl diglycol carbonate)) track detectors by carbon dioxide treatment

Nabil M. Hassan [a,b], Yuri Matai [b], Tamon Kusumoto [b], Yutaka Mori [b], Masato Kanasaki [b], Keiji Oda [b], Hisashi Kitamura [c], Teruaki Konishi [c], Satoshi Kodaira [c], Nakahiro Yasuda [d], Tomoya Yamauchi [b,*]

[a] *Department of Physics, University of Zagazig, Zagazig 44519, Egypt*
[b] *Graduate School of Maritime Sciences, Kobe University, 5-1-1 Fukaeminami-machi, Higashinada-ku, 658-0022 Kobe, Japan*
[c] *National Institute of Radiological Sciences, 4-9-1 Anagawa, Inage-ku, 263-8555 Chiba, Japan*
[d] *Research Institute of Nuclear Engineering, Fukui University, 1-2-4 Tetsuwachou, Tsuruga, Fukui 914-0047, Japan*

Abstract

The sensitization effect of carbon dioxide treatments with 0.6 MPa on poly(allyl diglycol carbonate) (PADC) etched track detectors by is confirmed for protons and He, C, and Fe ions, where the stopping powers range from 10 to 600 keV/μm. Based on the FT-IR study for the PADC films that were maintained at room temperature and at elevated temperatures, the diffusion coefficient of carbon dioxide, D, is determined as $D = 14670 \exp\left(-9030/T(K)\right)$ cm^2/s. The sensitivity is enhanced when carbon dioxide is released toward the chemical etching solution that passes through the detector surface. Segmented PADC polymer chains are washed away by the flow of carbon dioxide along the latent tracks in PADC, which results in a higher track etch rate.

Key words: PADC, ion track, sensitization, carbon dioxide, diffusion coefficient

Corresponding author: Tel +81-78-431-6307
E-mail address: yamauchi@martime.kobe-u.ac.jp

1. Introduction

Poly(allyl diglycol carbonate) (PADC) is a widely used solid-state nuclear track detector (SSNTD) in various branches of science and technology, such as cosmic ray studies, space dosimetry, neutron dosimetry, radiation biology, and nuclear physics (Cartwright et al., 1978, Nikezic and Yu, 2004). It is usually known by the trade name CR-39. Its registration sensitivity is sufficiently high to record recoiled protons by several 10 MeV neutrons (Oda et al., 2011). In addition to these conventional applications, it is also used in strengthened safeguard systems (Iguchi et al., 2005) and to detect ions in mixed fields in intense laser-driven ion acceleration experiments (Fukuda et al., 2009). PADC and other SSNTD materials are also used to estimate the concentration of radon/thoron in the environment (Hassan et al., 2009). Fig. 1 shows a repeat unit of PADC, which has an ether bond in the center and two carbonate ester bonds, which are composed of C=O and C-O-C in symmetric positions. Through a series of FT-IR spectral studies that were conducted on these units before and after the exposing to protons, heavy ions, and gamma rays, the units have been confirmed to be radiation-sensitive and easily broken at the C-O bonds (Yamauchi, 2003; Yamauchi et al., 2005, 2008; Mori et al., 2009, 2011, 2012). The repeated unit of the PADC detector combines via the polyethylene-like polymer chain at both ends, which is produced during the polymerization, as shown in Fig. 1. These units are relatively radiation-tolerant. When a PADC detector is irradiated with heavy ions, latent tracks are produced along the heavy ion trajectories. The core radii of the latent tracks in PADC are within several nm, depending on the ion species and their energies (Enge, 1995; Mori et al, 2011). After chemical etching, the latent tracks are enlarged and observed under an optical microscope as etch pits. The track formation is characterized with the detector registration sensitivity S, which is defined as the follows;

$$S = V - 1 = V_t / V_b - 1, \quad (1)$$

where V is the etch rate ratio of the track etch rate V_t, which is the etching speed along the latent track, to the bulk etch rate V_b, which is the etching rate of the undamaged detector surface (Somogyi and Szalay, 1973).

The sensitization effects of carbon dioxide gas under a pressure of several atmospheres on PADC-type track detectors were first reported by Fujii et al., and this was followed by a comprehensive examination by Csige (Fujii et al., 1995, 1997; Csige et al., 1997). Because the post-irradiation sensitization was observed to be effective and convenient, it has been applied for neutron and radon dosimetry (Hulber and Selmeczi, 2005) and for the micromachining process that uses proton beams (Baradács et al., 2008). Nevertheless, the fundamental mechanism of the sensitivity enhancement, from which we could discover a method to control the response of PADC detectors, has not been resolved.

In our recent study, we have confirmed the sensitization effects on 0.9 mm thick PADC sheets, which were irradiated using alpha particles with energies less than 6.1 MeV (Yamauchi et al., 2009). The fading of the sensitization with time between the treatment and the etching was also noted for 6.1 MeV alpha particles and thinner detector films of 100 μm in thickness. The releasing behavior of carbon dioxide from the treated PADC films was also examined using FT-IR spectrometry. Significant sensitization was observed when the PADC sheets contain a certain amount of carbon dioxide during the chemical etching.

The present study intends to understand the mechanism of sensitization of PADC detectors by carbon dioxide treatment. The detectors were exposed to protons and He, C, and Fe ions before the treatment, which covered a wide range of the stopping power between 10 and 600 keV/μm. The diffusion behavior of carbon dioxide in PADC was studied using FT-IR

spectrometry at room and elevated temperatures. Numerical calculations on the diffusion were also performed using the experimentally obtained diffusion coefficient. The sensitivity was found to increase when carbon dioxide gas was released toward the chemical etching solution that passes through the detector surface.

2. Experimental method

The PADC detectors that were used throughout the present study were BARYOTRAK sheets (Fukuvi Chemical Industry, Japan), which were produced from highly purified monomer, with different nominal thicknesses of 0.9 mm and 100 μm. To assess the effect of the carbon dioxide treatment, the PADC sheets with a thickness of 0.9 mm were cut into pieces of 2.5 × 2.5 cm^2 in size. The sheets were exposed to C and Fe ions at the port of the biological irradiation room of the Heavy Ion Medical Accelerator in Chiba, HIMAC, of the National Institute of Radiological Sciences, NIRS. Proton and He ion irradiations were performed at the port of the medium-energy irradiation room of HIMAC (Yasuda et al., 2004). The irradiation conditions of the incident energy are listed in Table 1. The exposures were performed in air and at room temperature. The stopping powers for the protons and the heavy ions were calculated using the SRIM code (Ziegler, 2004).

The carbon dioxide treatment was performed in a stainless steel chamber, which was connected to a carbon dioxide cylinder with a pressure regulator and to a rotary pump. Prior to the introduction of carbon dioxide gas, the chamber room with the samples was evacuated to below a few Pa. Then, the samples were exposed to the carbon dioxide gas that was introduced into the treatment chamber. The treatment process was performed at room temperature and at a pressures of 0.6 MPa for 1 week. After the treatment process finished, chemical etching was

started within 5 min. Chemical etching was performed in a 6 M KOH solution that was maintained at 70°C. The etched tracks were observed under an optical microscope (OLYMPUS BX60-F3), which was operated by a PC with the Win ROOF Ver. 5.04 image processor (MITANI Corporation, Japan).

The FT-IR measurements were performed to estimate the amount of carbon dioxide in the thin PADC sheets with a nominal thickness of 100 μm (FTIR-8400S, SHIMADZU, Japan). To trace the diffusion process after the treatment, the measurements were repeated for each sheet with sufficient time intervals depending on the temperatures. To evaluate the diffusion coefficient of carbon dioxide in PADC at elevated temperatures, the sheets were immersed in distilled water with temperatures of 60, 70, 80 and 90°C during the intervals. Immediately before each measurement, the sheets were cooled in water at room temperature, and the excess water on the surface was carefully removed by blowing.

3. Results and discussion

3.1. Effect of carbon dioxide treatment

Fig. 2 shows the typical optical microscopic views for the etch pits of 193 MeV C ions, 5.99 MeV He ions, and 15.3 GeV Fe ions, with and without the carbon dioxide treatment. Figs. 2 (a) & (b) indicate the open mouths of the etch pits, and Figs. 2 (c) & (d) show the side views of the etch pits after 4 h of etching. The thickness of the removed layer was determined as G = 10.7 μm for them, using the observations on the etch pits of the fission fragments from a Cf-252 source on the PADC sheets, which had the same lot number and were etched simultaneously with each sample. It is apparent that the pit radius and the pit length are increased by the carbon dioxide treatment. The etched pit profiles are conical in shape, as shown in these photographs.

Thus, we can apply the following equations to obtain the etch rate ratio, *V*, which was derived under the assumption that the etch pit is conical:

$$V = \left\{1 + (r/G)^2\right\} \Big/ \left\{1 - (r/G)^2\right\}, \text{ and} \quad (2)$$

$$V = 1/\sin\delta, \quad (3)$$

where r is the radius of the etch pit opening, and δ is the cone angle of the etch pit. Both relations are identical and provide similar results. It was difficult to obtain the sensitivity of the C and He ions without carbon dioxide treatment using Eq. (3). The results are summarized in Table 1, which includes the sensitivity of the proton beams. The identical data are plotted in Fig. 3 as a function of the stopping power. In the case of 4.8 MeV protons, we could not observe any etch pits after the normal etching. With the carbon dioxide treatment, we could detect etch pits for the protons under microscopic observations. In practical use, the treatment is effective to lower the detection threshold of the PADC detector. In general, the sensitization effect is observed in the examined region of the stopping power between 10 and 600 keV/μm. The stopping power is not a universal parameter for the sensitivity of PADC detectors, as shown in this figure. In a recent study, it has been confirmed that the restricted energy loss (REL) with a cut-off energy of 200 eV is a suitable parameter to express the response of the PADC detector, where the higher-energy components of the secondary electrons are considered to make a smaller contribution to track formation above the cut-off (Kodaira et al., 2013). When the sensitization effect is substantiated for more types of heavy ions, REL might be a suitable parameter.

3.2. Diffusion of carbon dioxide in PADC

In our previous work, we observed a decrease in sensitization with the time after the treatment (Yamauchi et al., 2009). From the dependence of the fading speed on the thickness of

the sheets, the absorbed carbon dioxide was inferred to escape via diffusion. The diffusion coefficient of carbon dioxide in PADC at room temperature was assessed using a simple solution of the diffusion equation for a slab system and the temporal changes in the FT-IR spectra of the treated sheets. In the present work, we have determined the diffusion coefficient at elevated temperatures that corresponded to the etching process and at the room temperature.

Fig. 4 shows the FT-IR spectra of the carbon dioxide that was absorbed in the PADC film with a 141 μm thickness; the spectra are shown against the wavenumber at the indicated times after the treatment. The absorption peaks at approximately 2340 cm^{-1} are assigned to anti-symmetric vibrations. Some satellite peaks were observed, and the main peak was saturated at the early stage of the release. The IR spectra of carbon dioxide in PADC films were different in shape from those in the atmosphere because of the suppression of rotational motion in the films. We are certain that the spectra in Fig. 4 are the spectra of carbon dioxide that was dissolved in PADC. After 1806 min, there is no detectable carbon dioxide in PADC. According to Beer-Lambert law, the absorbance, A, is proportional to the concentration of the considered functional group, c, and the thickness of the sample, d, as:

$$A = \varepsilon c d, \tag{4}$$

where ε is the molar absorbance coefficient. Using a gas cell with CaF_2 windows, it was determined that ε = 1.741×10^4 $M^{-1}cm^{-1}$ for gaseous carbon dioxide, where the absorbance is represented by the area under the peak. In the present work, this value is simply applied for the carbon dioxide in the PADC detector.

The concentration of carbon dioxide, $c(x,t)$, in a PADC sheet with a thickness of d in air after the treatment should be expressed by the following one-dimensional diffusion equation with sufficient initial and boundary conditions:

$$\frac{\partial c(x,t)}{\partial t} = D\frac{\partial^2 c(x,t)}{\partial x^2}, \tag{5}$$

$$t = 0 : c(x,0) = c_0,\ 0 \le x \le d,$$

$$t > 0 : c(0,t) = c(d,t) = 0,$$

where D is the diffusion coefficient, and c_0 is the equilibrium concentration in the treatment chamber. The chamber is opened at $t = 0$. By solving this, we obtain the followings:

$$c(x,t) = \frac{4c_0}{\pi}\sum_{n=0}^{\infty}\frac{1}{2n+1}\sin\left\{\frac{(2n+1)\pi}{d}x\right\}\exp\left[-\left\{\frac{(2n+1)\pi}{d}\right\}^2 Dt\right]. \tag{6}$$

After long time storage in air, $Dt/d^2 > 0.025$, the above equation becomes,

$$c(x,t) = \frac{4c_0}{\pi}\sin\left(\frac{\pi}{d}x\right)\exp\left\{-\left(\frac{\pi}{d}\right)^2 Dt\right\}. \tag{7}$$

Then the averaged concentration in the sheet, $\bar{c}$, is described by,

$$\bar{c} = \frac{1}{d}\int_0^d c(x,t)dx = \frac{8c_0}{\pi^2}\exp\left\{-\left(\frac{\pi}{d}\right)^2 Dt\right\}. \tag{8}$$

Therefore, the IR absorbance, A, is written as,

$$A = \varepsilon\bar{c}d = \frac{8c_0}{\pi^2}\varepsilon d\exp\left\{-\left(\frac{\pi}{d}\right)^2 Dt\right\}. \tag{9}$$

Taking the natural logarithm of both sides of equation (9), we obtain the following expression:

$$\ln A = \ln\left(\frac{8c_0}{\pi^2}\varepsilon d\right) - \left(\frac{\pi}{d}\right)^2 Dt. \tag{10}$$

This relation indicates that the slope of the plot of $\ln A$ against $(\pi/d)^2 t$ is the diffusion coefficient.

Fig. 5 shows the plots of $\ln A$ against the normalized time after the treatment at room temperature, and those at the elevated temperatures are shown the inset. The diffusion

coefficients were derived from the slope of the fitted lines and plotted in logarithmic scale as a function of the inversed absolute temperature (Fig. 6). We can find the temperature dependence of the diffusion coefficient in the form of the Arrhenius equation as the follows:

$$D = 14670 \exp\left(-9030/T(K)\right) \text{ cm}^2/\text{s}. \quad (11)$$

Using Eq. (10) and the values of the intercepts in Fig. 5, we found that the equilibrium concentration in the treatment chamber at 0.6 MPa was $c_0 = (1.41 \pm 0.77) \times 10^{-4}$ mol/cm^3. Some numerical calculations have been made using the experimentally obtained diffusion coefficient. A computer program based on the difference method was used, which was developed to study the depth-distribution of radiation-induced oxidative damage in polymers (Seguchi et al., 1981, 1982; Yamauchi et al., 2003). Fig. 7 (a) indicates the changes in the concentration of carbon dioxide in PADC during the treatment at 0.6 MPa. It takes more than 1 month to reach the saturation level in the center of the detector with 0.9 mm thickness, which is consistent with the previous results that the bulk etch rate and the sensitivity gradually increased with treatment time even after one week (Yamauchi et al, 2009). Fig. 7 (b) shows the reduction in concentration in the PADC with a 145 μm thickness at an etching temperature of 70ºC. This result implies that the absorbed carbon dioxide completely diffused away from the detector within 1 h. This result is also consistent with our previous study on FT-IR measurement after the etching (Yamauchi et al, 2009). The diffusion model describes the behavior of carbon dioxide well for each detector thickness and each temperature.

Fig. 8 shows the flux of carbon dioxide on the detector surface with 0.9 mm thickness during the etching at 70ºC as a function of the etching time, and the inset shows the depth-distributions of the concentration. In the early stage, when the concentration in the center region is saturated, the flux is higher than 4.0×10^{14} molecules/cm^{2}s. Two hours after from the etching

started, the flux is approximately 2.3×10^{14} molecules/cm^{2}s. Let us compare these values with the etching rate of the detector. The bulk etch rate of PADC is approximately 2.1 μm/h in the present condition. Because the density and the molecular mass of PADC are 1.32 g/cm^3 and 274, respectively, each repeat unit occupies a volume of 3.45×10^{-10} μm^3. Therefore, on averaged, 1.7×10^{14} of the repeat unit of PADC is etched away per unit area of the surface per second (1.7×10^{14} units/cm^{2}s). The flux of carbon dioxide is compatible with the loss amount induced by the chemical etching. These estimations indicate that the flow of carbon dioxide can affect the etching rate, especially in the early stage of the etching and at the tips of the etch pits, where the gradient of the carbon dioxide concentration should be locally enhanced.

Recent FT-IR studies on the structural modification along the latent-tracks in polymers tell us that the dominant breaking point in PADC is the ether bonds and carbonate ester bonds (Yamauchi et al., 2005, 2008; Mori et al., 2009, 2011, 2012). Carbon dioxide and ethylene-like molecules will be produced from the sensitive part of PADC (see Fig. 1). A mass spectrometric study supports this view by detecting ethylene glycol in the etching solution, as well as diethylene glycol and polyallylalcohols in the etching solution (Kodaira et al., 2012). The ethylene glycol is detected only for the irradiated PADC. The products of the bulk etching were limited to diethylene glycol and polyallylalcohols because the attack of the hydroxide ion results in the hydrolysis of the carbonate ester bonds (Gruhn et al., 1980). A continuous flow of carbon dioxide can make it easier to remove smaller molecules such as ethylene glycol, which are formed at the tips of the etch pits. The carbon dioxide may wash the detector surface and bring segmented parts of PADC network into the etching solution, which enhances the track etching rate (Enge, 1995).

3.3. Bending etch pit

Based on the etching tests and the numerical calculation for the depth-distribution of carbon dioxide in the treated PADC sheets, we can hypothesize that the track etch rate was enhanced because the significant flow of carbon dioxide washed the detector surface during the chemical etching. The sensitization effects were lost when the absorbed carbon dioxide escaped outside the detector. To confirm this hypothesis, we performed two simple etching tests. In the first test, the chemical etching was conducted for 4 h with the carbon dioxide treatment, which was followed by 2 h of the normal etching. The normal etching was conducted after identifying the complete loss of the absorbed carbon dioxide using the FT-IR measurements. In the second experiment, the normal etching was performed for 6 h, which was followed by 1 h of the etching with sensitization. Figs. 9 (a) and (b) show the results of each etching test. The cone angle is apparently increased in the first experiment (Fig. 9 (a)). The sensitization effect vanished during the later normal etching. However, the cone angle is remarkably reduced in the second experiment (Fig. 9 (b)). These tests demonstrate that the sensitization will effectively work when the PADC detector contains a certain amount of carbon dioxide during the chemical etching.

4. Conclusion

The sensitization effect of the carbon dioxide treatments at 0.6 MPa on PADC track detectors was confirmed for protons and He, C, and Fe ions, for which the stopping powers range from 10 to 600 keV/μm. The detection threshold for protons was lowered by the treatment from 16.8 to 10.5 keV/μm. Based on the FT-IR study for PADC films that were maintained at room temperature and elevated temperatures, the diffusion coefficient and the saturation concentration of carbon dioxide within PADC were determined, which enables us to calculate the carbon

dioxide concentration as a function of both depth and time. The diffusion coefficient was $D = 14670 \exp\left(-9030/T(K)\right)$ cm^2/s. The behavior of carbon dioxide in the PADC films was well described by the diffusion model. We concluded that the sensitivity was enhanced when carbon dioxide was released toward the chemical etching solution that passes through the detector surface.

Acknowledgment

The authors would like to express their thanks and appreciation to the staff of NIRS-HIMAC and Mr. H. Fukao for their support during the experiments. This work was performed as a part of the research project with heavy ions at NIRS-HIMAC. This work was also supported by a grant-in-aid for scientific research C from the Japan Society for Promotion of Science. One of the authors (Nabil Hassan) is grateful to the Egyptian government for its financial support to him.

Reference

Baradács, E., Csige, I., Rajta, I., 2008. CO_2 treatment and vacuum effects in proton beam micromachining of PADC. Radiat. Meas. 43, 1354-1356.

Cartwright, B. G., Shirk, E. K., Price, P. B., 1978. A nuclear-track recording polymer of unique sensitivity and resolution. Nucl. Instrum. Meth. 153, 457-460.

Clark, J., 1975. The mathematics of diffusion. Clarendon Press, Oxford.

Csige, I., 1997. Post irradiation sensitization of CR-39 track detector in carbon dioxide atmosphere. Radiat. Meas. 28, 171-176.

Enge,W., 1995. On the question of nuclear track formation in plastic material. Radiat. Meas. 25, 11-26.

Fujii, M., Yokota, R., Kobayashi, T., Hasegawa, H., 1995. Sensitization of polymeric track detector with carbon dioxide. Radiat. Meas. 25, 141-144.

Fujii, M., Yokota, R., Kobayashi, T., Hasegawa, H., 1997. Effect of vacuum oxygen and carbon dioxide on the track registration in SR-90 and CR-39. Radiat. Meas. 28, 61-64.

Fukuda, Y., Faenov, A.Ya., Tampo, M., Pikuz, T. A., Nakamura, T., Kando, M., Hayashi, Y., Yogo, A., Sakaki, H., Kameshima, T., Pirozhkov, A. S., Ogura, K., Mori, M., Esirkepov, T. Zh., Koga, J., Boldarev, A. S., Gasilov, V. A., Magunov, A. I., Yamauchi, T., Kodama, R., Bolton, P. R., Kato, Y., Tajima, T., Daido, H., Bulanov S.V., 2009. Energy Increase in Multi-MeV Ion Acceleration in the Interaction of a Short Pulse Laser with a Cluster-Gas Target. Phys. Rev. Lett. 103, 165002.

Gruhn, T. A., Li, W. K., Benton, E. V., Cassou, R. M., Johonson, C. S., 1980. Etching mechanisms and behaviour of polycarbonates in hydroxide solution. In: Proc. 10th Int. Conf. Solids State Nucl. Track Detectors, 291-302.

Hassan, N.M, Hosoda, M., Ishikawa, T., Tokonami, S., Fukushi, M., Hafez, A.F., Khalil, E., 2009. ^{222}Rn Exhalation Rate from Egyptian Building Materials Using Active and Passive Methods. JpJ of Health Phys., 44, 106-111.

Hulber, E., Selmeczi, D., 2005. Counting recoil proton tracks on PADC without a pre-etching step. Anovel approach for neutron dosimeter application. Radiat. Meas. 40, 616-619.

Iguchi, K., Esaka, K.T., Lee, C.G., Inagawa, J., Esaka, F., Onodera, T., Fukuyama, H., Suzuki, D., Sakurai, S., Watanabe, K., Usuda S., 2005. Study on the etching conditions of polycarbonate detectors for particle analysis of safeguards environmental samples. Radiat. Meas. 40, 363-366.

Kodaira, S., Nanjo, D., Kawashima, H., Yasuda, N., Konishi, T., Kurano, M., Kitamura, H., Uchihori, Y., Naka, S., Ota, S., Ideguchi, Y., Hasebe, N., Mori, Y., Yamauchi, T., 2012. Mass spectrometry analysis of etch products from CR-39 plastic irradiated by heavy ions. Nucl. Instrum. Meth. B286, 229-232.

Kodaira, S., Yasuda, N, Konishi, T., Kitamura, H., Kurano, M., Kawashima, H., Uchihori, Y., Ogura, K., Benton:, E. R., 2013.Calibration of CR-39 with atomic force microscope for the measurement of short range tracks from proton-induced target fragmentation reactions Radiat. Meas. 50, 232-236.

Mori, Y., Ikeda, T., Yamauchi, T., Sakamoto, A., Chikada, H., Honda, Y., Oda, K., 2009. Radiation chemical yield for loss of carbonate ester bonds in PADC films exposed to gamma ray. Radiat. Meas. 44, 211-213.

Mori, Y., Yamauchi, T., Kanasaki, M., Maeda, Y., Oda, K., Kodaira, S., Konishi, T., Yasuda, N., Barillon, R., 2011. Radiation chemical yields for loss of ether and carbonate ester bonds in PADC films exposed to proton and heavy ion beams. Radiat. Meas, 46, 1147-1153.

Mori, Y., Yamauchi, T., Kanasaki, M., Hattori, A., Matai, Y., Matsukawa, K., Oda, K., Kodaira, S., Kitamura, H., Konishi, T., Yasuda, N., Tojo, S., Honda, Y., Barillon, R., 2012. Greater radiation chemical yields for losses of ether and carbonate ester bonds at lower stopping powers along heavy ion tracks in poly(allyl diglycol carbonate) films. Appl. Phy. Exp., 5, 086401.

Nikezic, D., Yu, K.N., 2004. Formation and growth of tracks in nuclear track materials. Mater. Sci. Eng. R 46, 51-123.

Oda, K., Hayano, D., Kajihara, M., Ohguchi, H., Yamauchi, T., Yamamoto, T., 2011. Control technique of personal dosemeter response to fast neutrons with multi-layer radiator. Radiat. Meas. 46, 1786-1789.

Seguchi, T., Hashimoto, S., Arakawa, K., Hayakawa, N., Kawakami, W., Kuriyama., I., 1981. Radiation induced oxidative degradation of polymers – I: Oxidation region in polymer films irradiated in oxygen under pressure. Radiat. Phys. Chem. 17, 195-201.

Seguchi, T., Arakawa, K., Hayakawa, N., Watanabe, Y., Kuriyama., I., 1982. Radiation induced oxidative degradation of polymers – II: Effects of radiation on swelling and gel fraction of polymer. Radiat. Phys. Chem. 17, 195-201.

Somogyi, G., Szalay, S.A., 1973. Track-diameter kinetics in dielectric track detectors. Nucl. Instr. Meth., 109, 211-232.

Yamauchi, T., 2003. Studies on the nuclear tracks in CR-39 plastics. Radiat Meas 36, 73-81.

Yamauchi, T., Somaki, Y., Nakai, H., Oda, K., Ikeda, T., Honda, H., Tagawa, S., 2003. Oxidative degradation of CR-39 track detector in the surface region during gamma-irradiation. Nucl. Instrum. Meth. B 208, 489-494.

Yamauchi, T., Barillon, R., Balanzat, E., Asuka, T., Izumi, K., Masutani, T., Oda, K., 2005. Yields of CO_2 formation and scissions at ether bonds along nuclear tracks in CR-39. Radiat Meas 40, 224-228.

Yamauchi, T., Watanabe, S., Seto, A., Oda, K., Yasuda, N., Barillon, R., 2008. Loss of carbonate ester bonds along Fe ion tracks in thin CR-39 films. Radiat. Meas. 43, S106-S110.

Yamauchi, T., Mori, Y., Chikada, H., Sakamoto, A., Kii, J., Kanasaki, M., Oda, K., Fujii, M., 2009. Sensitization of PADC track detector in carbon dioxide gas. Radiat. Meas. 44, 1105-1108.

Yasuda, N., Konishi, T., Matsumoto, K., Yamauchi, T., Asuka, T., Furusawaa, Y., Sato, Y., Oda, K., Tawara, H., Hieda, K., 2005. Dose distribution of carbon ions in air assessed using imaging plates and ionization chamber. Radiat. Meas. 40, 384-388.

Ziegler, J., F., 2004. SRIM-2003. Nucl. Instrum. Meth. B 219: 1027-1036.

Figures captions

Fig. 1 A repeat unit of the PADC detector.

Fig. 2 Microscopic views of the etch pits of 193 MeV C ions, 5.99 MeV He ions, and 15.3 GeV Fe ions: (a) the open mouth of the etch pits with the normal treatment, (b) the open mouth of the etch pits with CO_2 treatment, (c) the profile of the etch pit with the normal treatment, and (d) the profile of the etch pit with CO_2 treatment. Each lateral bar denotes 30 μm.

Fig. 3 Changes in the response of the PADC detectors for protons and heavy ions with and without CO_2 treatment.

Fig. 4 Changes in the FT-IR spectra of carbon dioxide in the PADC detector with 141 μm thickness after the CO_2 treatment.

Fig.5 Reduction of the absorbance of carbon dioxide in the PADC detector at several temperatures against the normalizing time after the CO_2 treatment. The slope of the fitted lines corresponds to the diffusion coefficient of carbon dioxide in PADC at each temperature.

Fig.6 Diffusion coefficient of carbon dioxide in the PADC detector as an inverse function of the temperature.

Fig.7 Changes in the depth-distribution of carbon dioxide in the PADC detector, which were assessed using numerical calculations: (a) during the CO_2 treatment with a thickness of 0.9 mm, it takes more than 6 weeks to be saturated, (b) during the chemical etching at 70^{o}C with a thickness of 145 μm, carbon dioxide is diffused away within 1 h.

Fig. 8 Flux of carbon dioxide on the surface of the PADC detector with a thickness of 0.9 mm during the chemical etching at 70^{o}C.

Fig. 9 Bending etch pits for 6.1 MeV He ions: (a) Etching with CO_2 treatment for 4 h was followed by 2 h of normal etching (the cone angle was increased), (b) Normal etching for 6 h was followed by 1 h of etching with CO_2 treatment (the cone angle was clearly sharpened).

Table 1 Irradiation conditions and detector sensitivity

Ions	Energy (MeV)	Stopping power ($keV\mu m^{-1}$)	Sensitivity (*V*-1)	
			Untreated(air)	Treated with CO_2
Iron	5710	599	3.59 ± 0.68	6.95 ± 1.85
	9660	413	2.64 ± 0.27	5.53 ±0.92
	15350	309	1.53 ± 0.22	3.51 ± 0.30
	18850	276	1.32 ± 0.14	3.10 ± 0.40
	21680	257	1.22 ± 0.11	2.10 ± 0.16
Carbon	193	142	0.29 ± 0.12	1.13 ± 0.16
	377	82	0.11 ± 0.02	0.81 ± 0.08
	446	71	0.08 ± 0.02	0.67 ± 0.15
	507	64	0.07 ± 0.01	0.61 ± 0.09
	562	59	0.05 ± 0.01	0.40 ± 0.10
Helium	0.79	276	1.66 ± 0.25	5.13 ± 1.13
	5.32	110	0.64 ± 0.08	3.04 ± 0.52
	5.99	101	0.53 ± 0.05	1.78 ± 0.10
	12.42	60	0.14 ± 0.01	0.77 ± 0.04
Proton	1.81	21.9	0.012 ± 0.003	0.072 ± 0.011
	2.23	18.9	0.010 ± 0.002	0.049 ± 0.008
	2.6	16.8	0.005 ± 0.001	0.030 ± 0.005
	4.8	10.5	ND*	0.018 ± 0.004

ND* none detected value

Table 2 Diffusion coefficient of CO_2 in the PADC detector at room temperature and at elevated temperatures

Temperature (^oC)	Diffusion Coefficient (cm^2/s)
25	8.7×10^{-10}
60	3.3×10^{-8}
70	6.3×10^{-8}
80	1.1×10^{-7}
90	1.8×10^{-7}

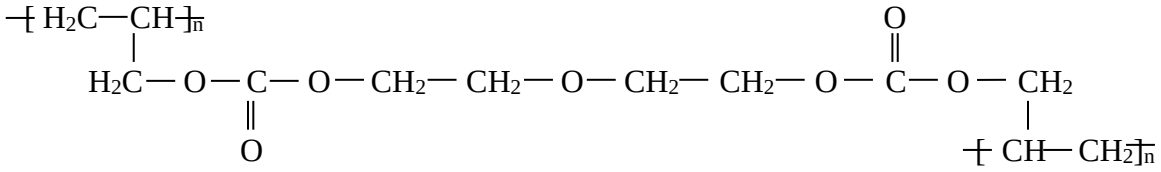

Fig. 1.

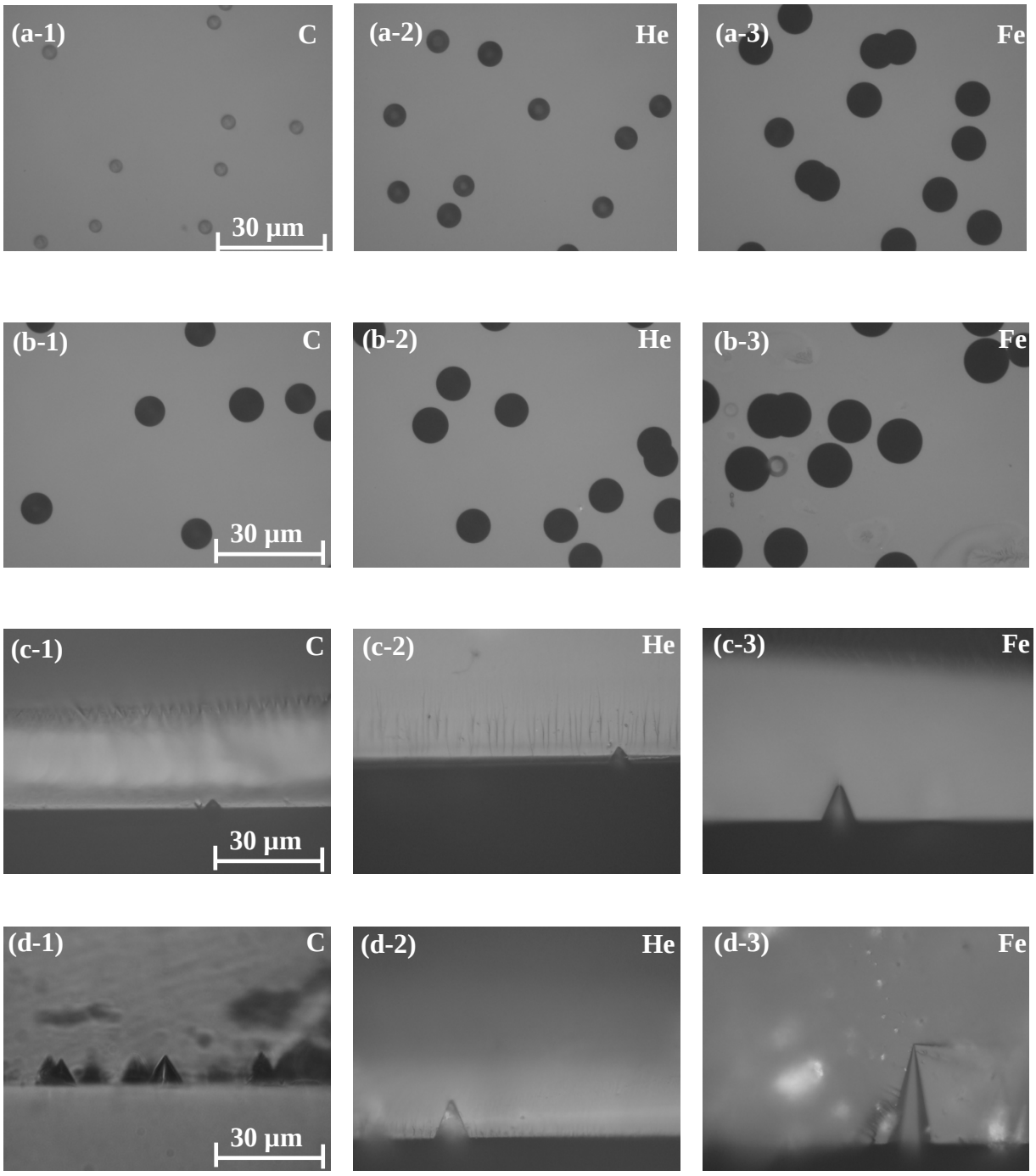
(a-1)
C
30 µm
(a-2)
He
(a-3)
Fe
(b-1)
C
30 µm
(b-2)
He
(b-3)
Fe
(c-1)
C
30 µm
(c-2)
He
(c-3)
Fe
(d-1)
C
30 µm
(d-2)
He
(d-3)
Fe

Fig. 2.

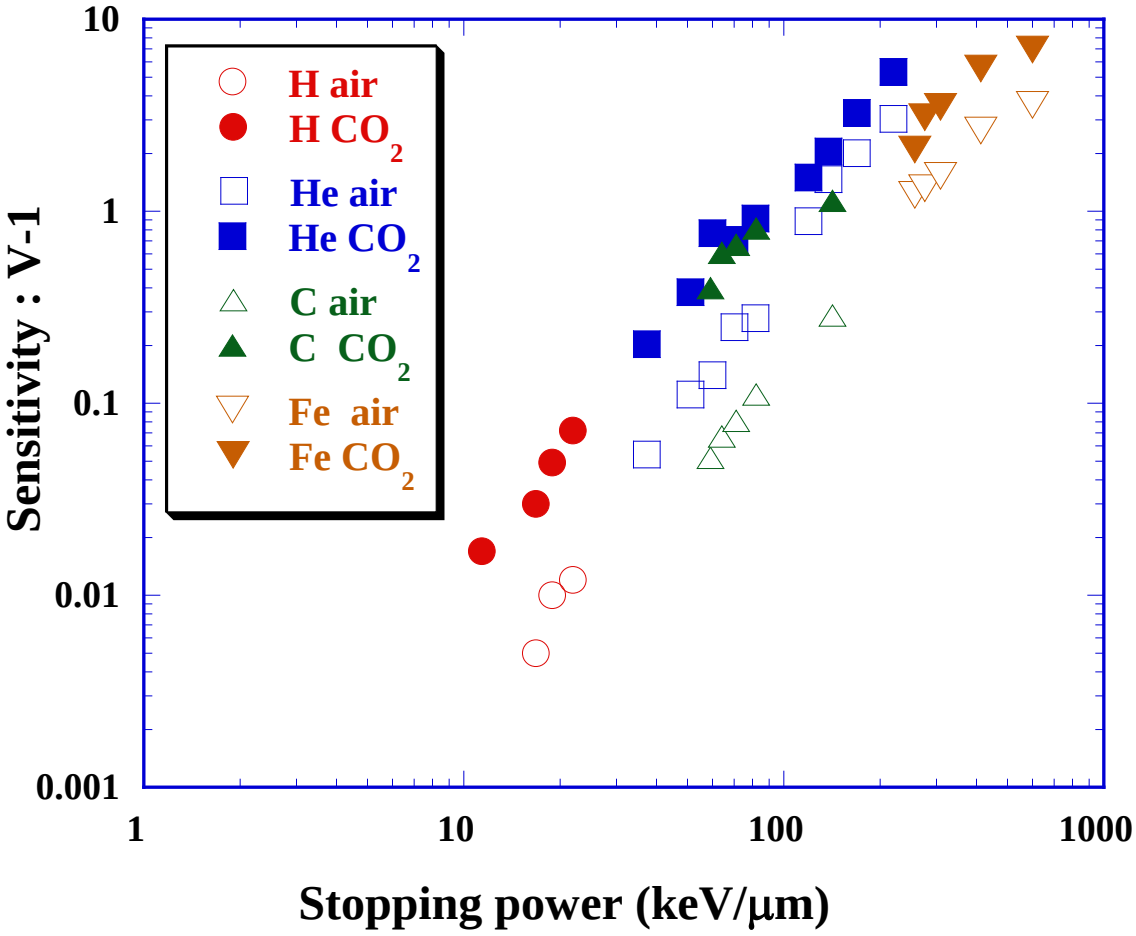
10
1
0.1
0.01
0.001
Sensitivity : V-1
1
10
100
1000
Stopping power (keV/μm)
H air
H CO2
He air
He CO2
C air
C CO2
Fe air
Fe CO2

Fig. 3.

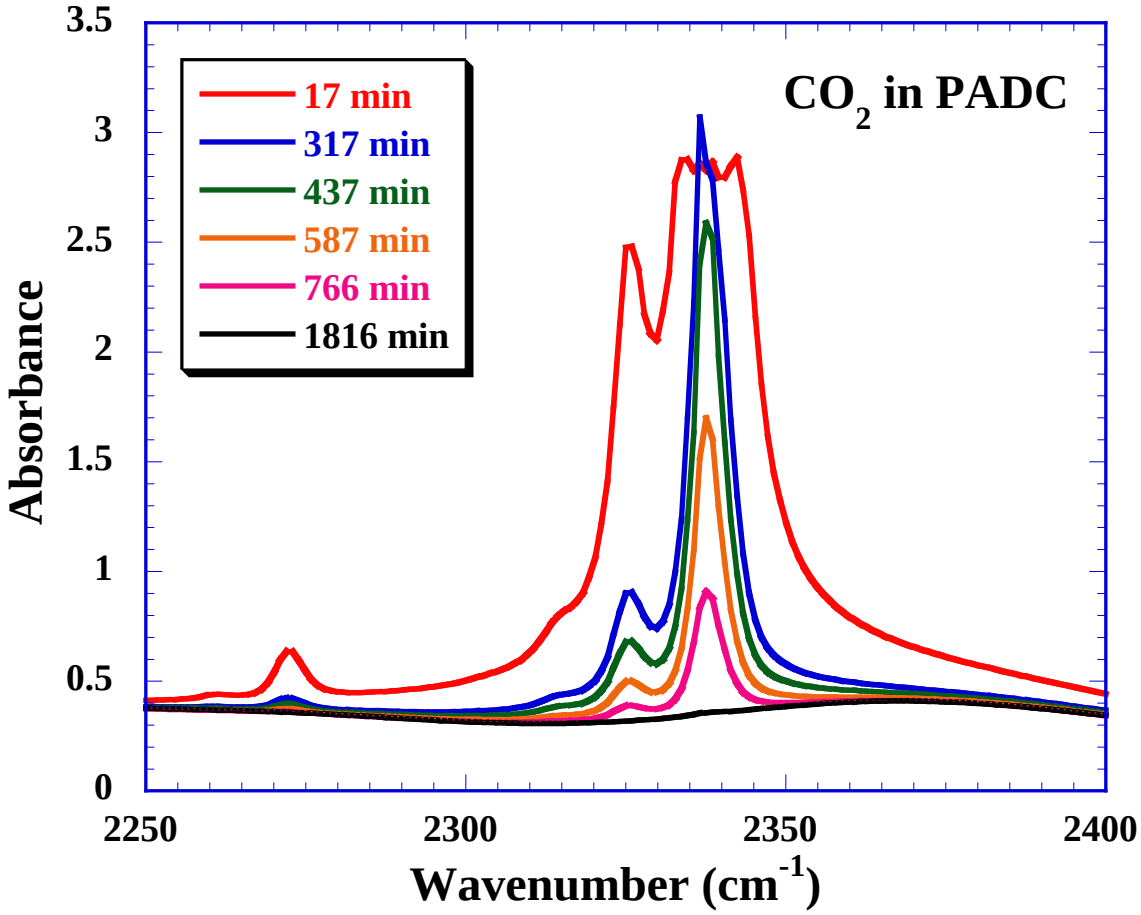
3.5
3
2.5
2
1.5
1
0.5
0
Absorbance
2250
2300
2350
2400
Wavenumber (cm-1)
17 min
317 min
437 min
587 min
766 min
1816 min
CO2 in PADC

Fig. 4.

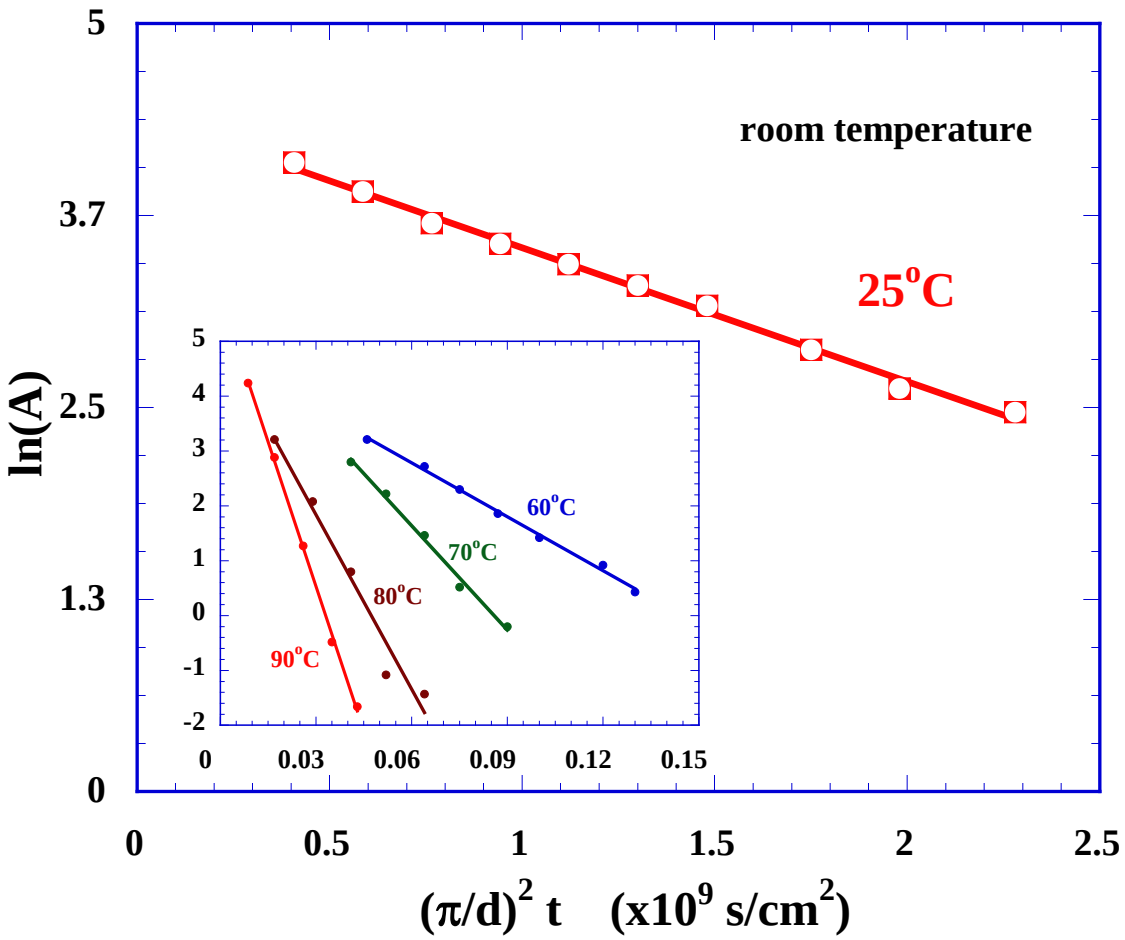
room temperature
25°C
60°C
70°C
80°C
90°C
ln(A)
(π/d)² t (x10⁹ s/cm²)
0
1.3
2.5
3.7
5
0.5
1
1.5
2
2.5
-2
-1
0.03
0.06
0.09
0.12
0.15
4

Fig. 5.

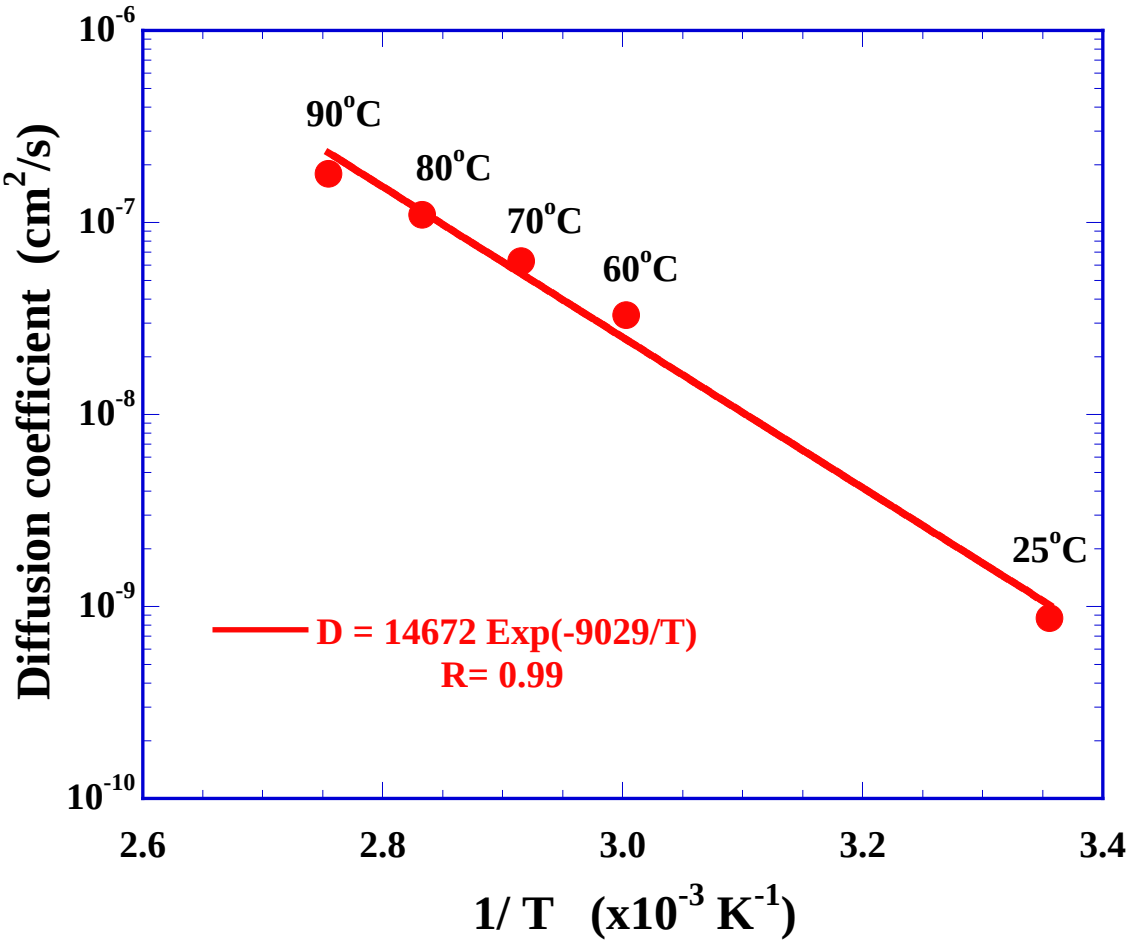
Diffusion coefficient (cm²/s)
10⁻⁶
10⁻⁷
10⁻⁸
10⁻⁹
10⁻¹⁰
90°C
80°C
70°C
60°C
25°C
D = 14672 Exp(-9029/T)
R= 0.99
2.6
2.8
3.0
3.2
3.4
1/ T (x10⁻³ K⁻¹)

Fig. 6.

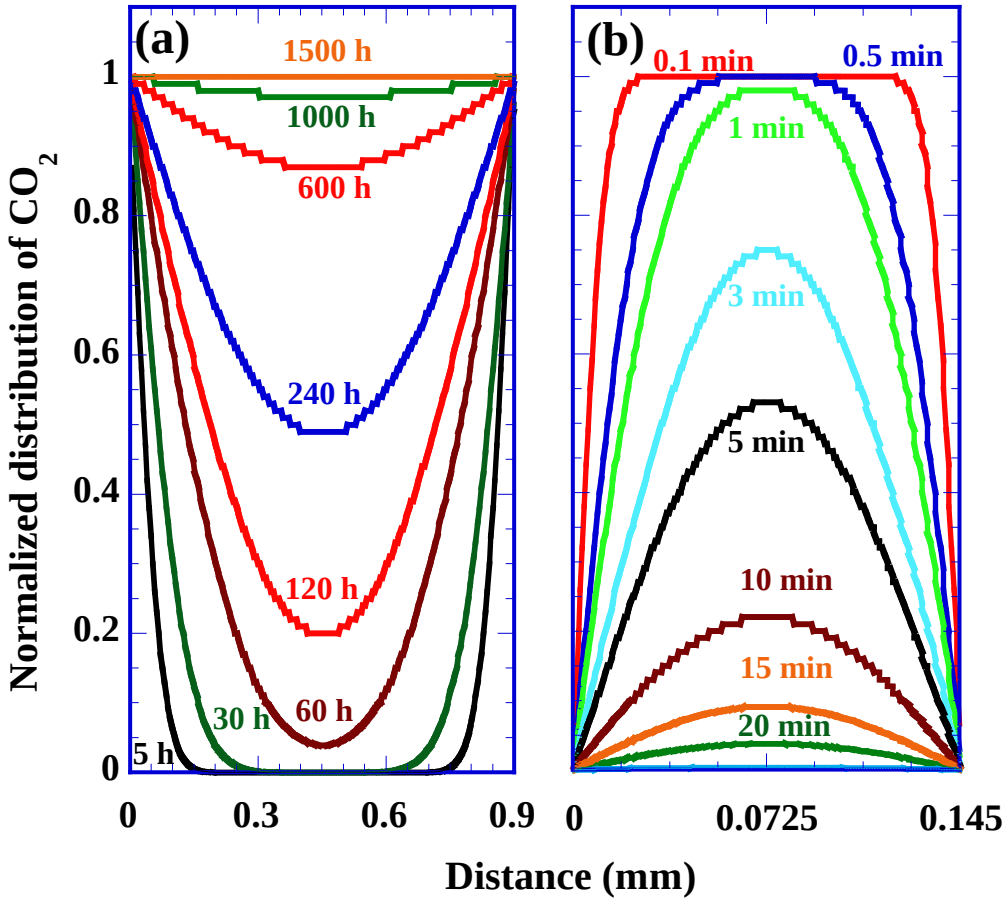
(a)
1500 h
1000 h
600 h
240 h
120 h
60 h
30 h
5 h
(b)
0.1 min
0.5 min
1 min
3 min
5 min
10 min
15 min
20 min
Normalized distribution of CO2
Distance (mm)
0
0.3
0.6
0.9
0.0725
0.145
0.2
0.4
0.8
1

Fig. 7.

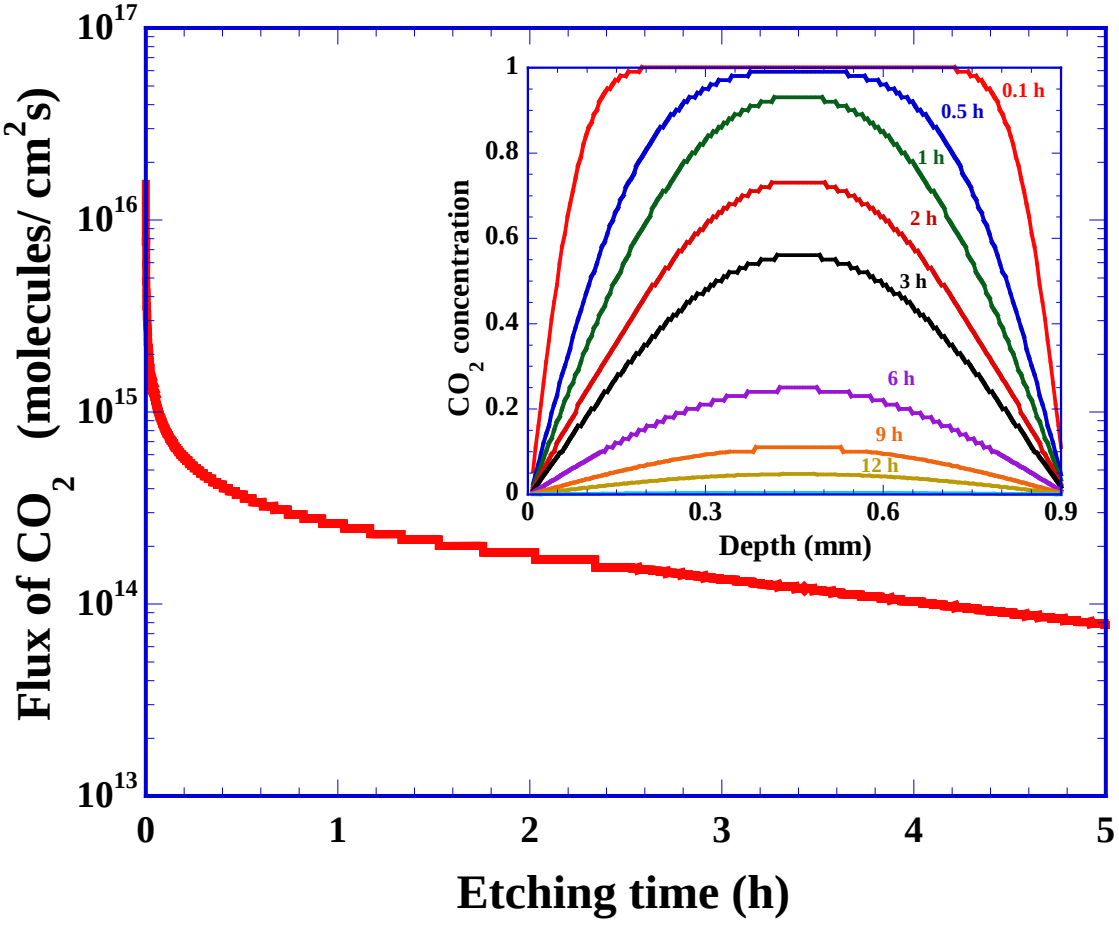
Flux of CO2 (molecules/ cm2s)
Etching time (h)
CO2 concentration
Depth (mm)
0.1 h
0.5 h
1 h
2 h
3 h
6 h
9 h
12 h

Fig. 8.

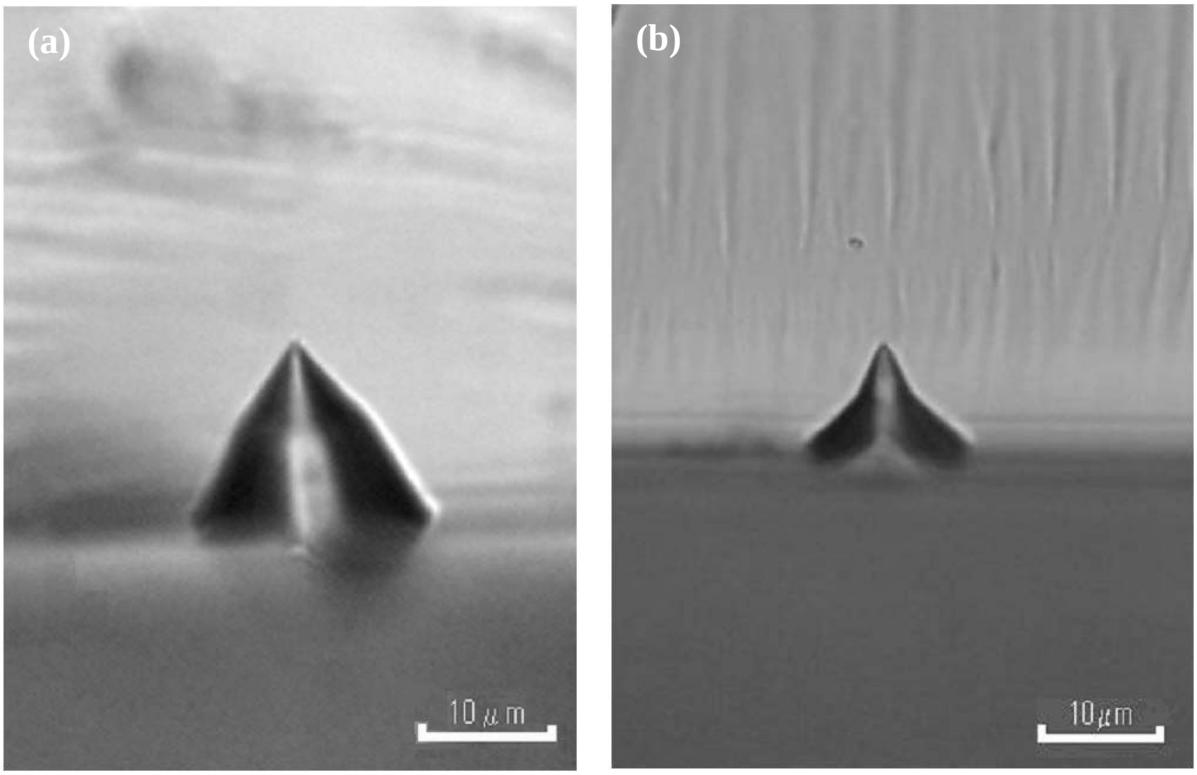

Fig. 9.